A unified formulation to assess multilayered theories for piezoelectric plates

D. Ballhause, M. d'Ottavio, B. Kröplin, E. Carrera

HAL Id: hal-01367092

https://hal.science/hal-01367092

Submitted on 10 Jan 2019

A unified formulation to assess multilayered theories for piezoelectric plates

D. Ballhause, M. D'Ottavio, B. Kröplin, E. Carrera

1. Introduction

Because of their self-monitoring and self-adaptive capability, so-called advanced intelligent structures have attracted considerable research over the past few years.

These structures have some distinct advantages over conventional actively controlled structures. Since intelligent structures are characterized by distributed actuation and sensing systems, more accurate response monitoring and control are possible. Some of the most significant work has concentrated on the development and implementation of actuators and sensors made of piezoelectric materials. Since Curie brothers [1], it is known that there are two basic phenomena 'direct and converse effects', characteristic of piezoelectric materials,

_____

* Corresponding author. Tel.: +39 11 5646836; fax: +39 11 5646899.

E-mail addresses: ballhause@isd.uni-stuttgart.de (D. Ball-hause), erasmo.carrera@polito.it (E. Carrera).

which permit them to be used as sensors and actuators. Although piezoelectricity has a long history, its use in actuation and control of light flexible structures for aerospace applications is relatively new. Overview papers are those by Rao and Sunar [2], Chopra [3], Tani et al. [4], and Sunar and Rao [5]. In most of these applications, the piezoelectric materials are used as sensor/actuator layers by embedding them in a multilayered structure which is often made by advanced anisotropic composite materials.

As pointed out by the already mentioned overview papers, the most important problems arising in the design of intelligent structures embedding piezo-layers are manufacturing, electro-mechanical modeling, optimization and control. Among these, the attention is herein focused on plate theories for the electro-mechanical modeling of flat, intelligent structures. The accurate description of mechanical and electrical fields in the layers is, in fact, essential in order to both perform a realistic simulation of direct/converse effect and prevent failure mechanisms of the structure.

The main issue of multilayered piezoelectric constructions is related to the possibility of exhibiting different mechanical–electrical properties in the thickness direction. In addition, anisotropic multilayered composites often exhibit both higher transverse shear and transverse normal flexibilities, with respect to in-plane deformability, than traditional isotropic one-layered ones. As a consequence, plate theories which are based on the extension of so-called Kirchhoff (or Classical Lamination Theory, CLT) and Reissner–Mindlin (or First order Shear Deformation Theory, FSDT) hypotheses can be ineffective to trace static and dynamic response of piezoelectric plates. Higher transverse deformabilty demands the inclusion of transverse shear and normal stresses which are discarded in classical analyses. Furthermore, transverse discontinuous mechanical properties cause displacement fields $\boldsymbol{u} = (u_x, u_y, u_z)$ which can exhibit a rapid change of their slopes in the thickness direction in correspondence to each layer interface. This is known as the *Zig-Zag* (ZZ) effect. Nevertheless, equilibrium reasons require *Interlaminar Continuity* (IC) for transverse stresses $\boldsymbol{\sigma}_n = (\sigma_{xz}, \sigma_{yz}, \sigma_{zz})$. A discussion on theories addressing ZZ and IC has been recently provided by Carrera [6]. As far as electrical variables are concerned, it should be noticed that in order to include a correct description of electrical stiffnesses, the electric field should have at least a linear distribution in thickness direction of the piezo-layers. As a consequence, at least a parabolic assumption for the electric potential into the layers is required.

Many refined plate theories have been proposed and extended to the electro-mechanical fields. A few examples are mentioned in the following text. Applications of CLT and FSDT to piezoelectric plates were given by Tiersten, [7] and Mindlin [8]. As example of a refined theory the work by Yang and Yu [9] is mentioned. The

electric fields generated by stresses, e.g. electrical stiffness, were not considered in these three works. The electro-mechanical coupling was indeed retained in following articles. Mitchell and Reddy [10] introduced a layer-wise (LW) description for the electric potential, while an equivalent single layer (ESL) description was retained for displacements. According to Reddy [11], it is intended that the number of displacement variables is kept independent of the number of constitutive layers in the ESL models, while the same variables are independent in each layer for LW cases. Refined ESL models have been discussed by Benjeddou [12]. ESL formulation taking into account ZZ and IC have been discussed by Touratier and Ossadzow-David [13]. A more complete discussion of the several contributions on electromechanical models of multilayered plates embedding piezo-layers, has been covered by recent exhaustive state-of-the-art articles. Interested readers are addressed to the review papers by Saravanos and Heyliger [14] and by Benjeddou [15].

However, most of the articles proposing refined theories for piezoelectric plates restricted the numerical comparison to classical plate theories, such as CLT and FSDT, and to available 3D solutions. Only in some cases other refined theories were included in the verification of the new method. Such a restriction does not permit to give a complete overview and assessment of available theories. The present work aims to contribute to this matter by enlarging the number of the theories available for a single problem: about thirteen theories are, in fact, implemented and compared for different test cases. The most accurate ones coincide with a layer-wise theory based on a fourth order expansion in each layer (LD4). Such a theory leads to a quasi-3D description of mechanical and electrical fields in the layers. The less accurate one coincides with CLT. Eleven further formulations with accuracies lying between LD4 and CLT are proposed and compared. These theories are able to cover many of the aspects characterizing 2D axiomatic theories for multilayered plates, such as ZZ, transverse shear deformation, transverse shear strains effects and to compare LW and ESL description.

In order to meet the mentioned proposals this paper reconsiders recent findings by Carrera [16–19]. In these papers a 'unified formulation' was proposed, basing on applications of the Principle of Virtual Displacement (PVD) and Reissner' Mixed Variational Theorem (RMVT) to mechanical problems. This *unified formulation* permits to derive governing equations in terms of a few *fundamental nuclei* whose expressions do not change by varying the assumptions made for the displacement variables in the layer thickness. In this work, these methods are extended to electro-mechanical static and dynamic analyses of multilayered plates embedding piezo-layers. Developments have been restricted to PVD applications. Layer-wise and equivalent single layer

models with linear up to fourth-order expansion in the plate thickness (z-direction) have been implemented. Zig-zag effects are described by means of the Murakami zig-zag function [20]. Transverse normal strain effects have also been considered. As far as the electrical potential is concerned, attention has been restricted to a layer-wise description. Results are given for the case of orthotropic layers and simply supported plates loaded by harmonic distributions of mechanical and electrical loadings. Numerical results are given for both free vibration and static response. Verification is made with respect to available 3D solutions and an assessment of various plates theories is finally given.

2. Preliminary

A multilayered flat plate consisting of N_L layers, which can be piezoelectric or purely elastic is examined. The laminae are considered homogeneous and perfectly bonded with each other. The notation and the Cartesian coordinate system x, y, z referred to the middle surface can be seen in Fig. 1. The plate has the length a, width b and height h. The index k is used for the layer number. The local thickness coordinate of the layer is z_k, the non-dimensional correspondent is $\zeta_k = (2z_k/h_k)$. The linear elastic range of the materials and the physical limits of the piezoelectric layer, like Curie temperature and depolarization potential, are not exceeded by any deformations or loadings. The stresses and strains are represented in engineering notation with the indices 11, 22, 33, 13, 23, and 12. The stiffness coefficients $\widetilde{C}_{ij}$ refer to these with $i, j = 1 \ldots 6$. The directions of the piezoelectric material are named in the standard manner with 1–3, axis 3 being the polarization direction of the material. The polarization axis is assumed parallel to the thickness direction z of the plate. To establish a uniform modeling, all layers in the laminate are assumed to be piezoelectric, where for purely elastic layers the piezoelectric coefficients are set to zero.
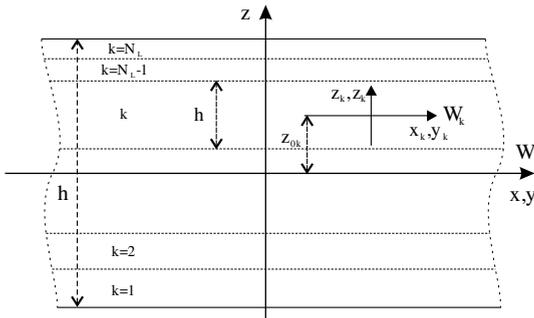
Fig. 1. Geometry and notations of multilayered plate.

2.1. Constitutive equations

The coupling between the stresses and the electric field in the k-layer is sustained by the direct and converse piezoelectric effect and is represented, according to the IEEE standard [21] with the following constitutive equations in array form:

$$\boldsymbol{\sigma}^k = \widetilde{\boldsymbol{C}}^k \boldsymbol{\epsilon}^k - \boldsymbol{e}^{k\mathrm{T}} \boldsymbol{E}^k \tag{1}$$

$$\widetilde{\boldsymbol{D}}^k = \boldsymbol{e}^k \boldsymbol{\epsilon}^k + \boldsymbol{\varepsilon}^k \boldsymbol{E}^k \tag{2}$$

Boldfaced letters are used for arrays, superscript T denotes transposition. The vectors $\boldsymbol{\sigma}$ and $\boldsymbol{\epsilon}$ contain the six stress and strain components, respectively. $\widetilde{\boldsymbol{D}}^k$ is the dielectric displacement and $\boldsymbol{E}^k$ the electric field strength with three direction components each

$$\widetilde{\boldsymbol{D}}^k = \left[\widetilde{D}_1^k, \widetilde{D}_2^k, \widetilde{D}_3^k \right]^{\mathrm{T}} \quad \boldsymbol{E}^k = \left[E_1^k, E_2^k, E_3^k \right]^{\mathrm{T}} \tag{3}$$

The [6 × 6] array $\widetilde{\boldsymbol{C}}^k$ contains the elastic, the [3 × 6] array $\boldsymbol{e}^k$ the piezoelectric and finally the [3 × 3] array $\boldsymbol{\varepsilon}^k$ the dielectric coefficients of the k-th layer. For convenience the stresses and strains are separated into in-plane and transverse components, denoted respectively with p and n as follows:

$$\boldsymbol{\sigma}_p^k = \left[\sigma_{11}^k, \sigma_{22}^k, \sigma_{12}^k \right]^{\mathrm{T}} \quad \boldsymbol{\sigma}_n^k = \left[\sigma_{13}^k, \sigma_{23}^k, \sigma_{33}^k \right]^{\mathrm{T}} \tag{4}$$

$$\boldsymbol{\epsilon}_p^k = \left[\epsilon_{11}^k, \epsilon_{22}^k, \epsilon_{12}^k \right]^{\mathrm{T}} \quad \boldsymbol{\epsilon}_n^k = \left[\epsilon_{13}^k, \epsilon_{23}^k, \epsilon_{33}^k \right]^{\mathrm{T}} \tag{5}$$

The array formulation Eq. (1) of the constitutive equations can then be rewritten as

$$\begin{aligned}
\boldsymbol{\sigma}_p^k &= \widetilde{\boldsymbol{C}}_{pp}^k \boldsymbol{\epsilon}_p^k + \widetilde{\boldsymbol{C}}_{pn}^k \boldsymbol{\epsilon}_n^k - \boldsymbol{e}_p^{k\mathrm{T}} \boldsymbol{E}^k \\
\boldsymbol{\sigma}_n^k &= \widetilde{\boldsymbol{C}}_{pn}^{kT} \boldsymbol{\epsilon}_p^k + \widetilde{\boldsymbol{C}}_{nn}^k \boldsymbol{\epsilon}_n^k - \boldsymbol{e}_n^{k\mathrm{T}} \boldsymbol{E}^k \\
\widetilde{\boldsymbol{D}}^k &= \boldsymbol{e}_p^k \boldsymbol{\epsilon}_p^k + \boldsymbol{e}_n^k \boldsymbol{\epsilon}_n^k + \boldsymbol{\varepsilon}^k \boldsymbol{E}^k
\end{aligned} \tag{6}$$

The arrays of the elastic material properties for monoclinic material systems explicitly read

$$\widetilde{\boldsymbol{C}}_{pp}^k = \begin{bmatrix} \widetilde{C}_{11}^k & \widetilde{C}_{12}^k & \widetilde{C}_{16}^k \\ \widetilde{C}_{12}^k & \widetilde{C}_{22}^k & \widetilde{C}_{26}^k \\ \widetilde{C}_{16}^k & \widetilde{C}_{26}^k & \widetilde{C}_{66}^k \end{bmatrix} \quad \widetilde{\boldsymbol{C}}_{pn}^k = \begin{bmatrix} 0 & 0 & \widetilde{C}_{13}^k \\ 0 & 0 & \widetilde{C}_{23}^k \\ 0 & 0 & \widetilde{C}_{36}^k \end{bmatrix}$$

$$\widetilde{\boldsymbol{C}}_{nn}^k = \begin{bmatrix} \widetilde{C}_{55}^k & \widetilde{C}_{45}^k & 0 \\ \widetilde{C}_{45}^k & \widetilde{C}_{44}^k & 0 \\ 0 & 0 & \widetilde{C}_{33}^k \end{bmatrix}$$

The arrays of the piezoelectric constants for monoclinic material are

$$\boldsymbol{e}_p^k = \begin{bmatrix} 0 & 0 & 0 \\ 0 & 0 & 0 \\ e_{31}^k & e_{32}^k & e_{36}^k \end{bmatrix} \quad \boldsymbol{e}_n^k = \begin{bmatrix} e_{14}^k & e_{15}^k & 0 \\ e_{24}^k & e_{25}^k & 0 \\ 0 & 0 & e_{33}^k \end{bmatrix}$$

The piezoelectric materials considered in this work are all transversally isotropic to the 3-direction. Thus the components e_{14}, e_{25} and e_{36} become zero. The permittivity coefficients are combined to the array

$$\boldsymbol{\varepsilon} = \begin{bmatrix} \varepsilon_{11} & \varepsilon_{12} & 0 \\ \varepsilon_{21} & \varepsilon_{22} & 0 \\ 0 & 0 & \varepsilon_{33} \end{bmatrix}$$

Attention has been herein restricted to the case $\varepsilon_{12} = \varepsilon_{21} = 0$ which corresponds to hexagonal crystal systems, see [21].

2.2. Geometric relations

The strains $\boldsymbol{\epsilon}_p^k$ and $\boldsymbol{\epsilon}_n^k$ are related to the displacements $\boldsymbol{u}^k = [u_x^k, u_y^k, u_z^k]^{\mathrm{T}}$ according to the linear geometrical relations

$$\boldsymbol{\epsilon}_p^k = \boldsymbol{D}_p \boldsymbol{u}^k \quad \boldsymbol{\epsilon}_n^k = \boldsymbol{D}_n \boldsymbol{u}^k \tag{7}$$

The arrays $\boldsymbol{D}_p$ and $\boldsymbol{D}_n$ contain the differential operators. The definition of the electric field strength $\boldsymbol{E}^k$ according to the Maxwell equations is given by

$$\boldsymbol{E}^k = \boldsymbol{D}_e \Phi^k \tag{8}$$

The explicit form of the introduced linear differential operators arrays read

$$\boldsymbol{D}_p = \begin{bmatrix} \partial_x & 0 & 0 \\ 0 & \partial_y & 0 \\ \partial_y & \partial_x & 0 \end{bmatrix} \quad \boldsymbol{D}_n = \begin{bmatrix} \partial_z & 0 & \partial_x \\ 0 & \partial_z & \partial_y \\ 0 & 0 & \partial_z \end{bmatrix}$$

$$\boldsymbol{D}_e = \begin{bmatrix} -\partial_x & 0 & 0 \\ 0 & -\partial_y & 0 \\ 0 & 0 & -\partial_z \end{bmatrix}$$

wherein ∂_α denotes partial derivation with respect to the α-coordinate.

3. Unified formulation

The key point of the unified formulation is the usage of generalized assumptions for the displacements $\boldsymbol{u}$ and, in the piezoelectric case, also for the potential Φ. In the following section, these assumptions are defined and the possible theories are listed.

3.1. Assumptions for displacement

The generalized assumptions for the displacement $\boldsymbol{u} = [u_x, u_y, u_z]^{\mathrm{T}}$ with the given number of expansion N are

$$\boldsymbol{u} = F_t \boldsymbol{u}_t + F_r \boldsymbol{u}_r + F_b \boldsymbol{u}_b = F_\tau \boldsymbol{u}_\tau$$
$$\text{where } \tau = t, b, r \quad \text{and} \quad r = 1, 2, \ldots, N \tag{9}$$

The displacement is separated into a set of thickness functions F_τ and the correspondent displacement vari-
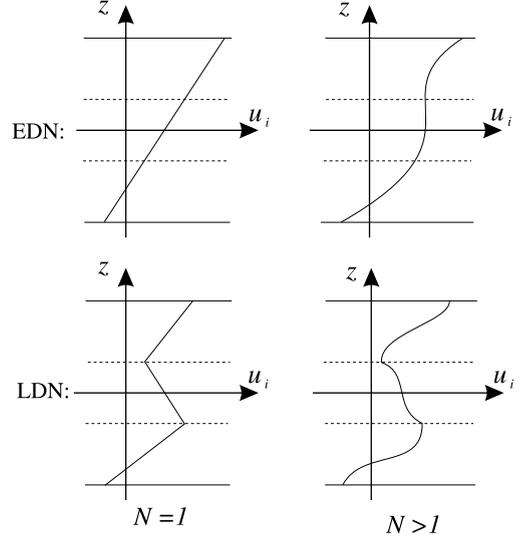
Fig. 2. Displacement assumptions of ESL and LW model.

ables $\boldsymbol{u}_\tau$. This formulation incorporates a wide variety of different theories with the same basic arrays for the governing equations (fundamental nuclei). The two basic concepts are layer-wise (LW) and equivalent single layer (ESL) modeling. In the first case different displacement variables are assumed for every layer, while in the second case only one set of displacement variables for the whole plate is defined. Fig. 2 shows from a qualitative point of view the differences between LW and ESL descriptions with linear ($N = 1$) or higher-order expansions for a three layer problem For convenience the two modelings (LW and ESL) have been in Fig. 2 denoted by LDN ed EDN, according to the acronyms that will be clarified below.

3.1.1. ESL model with Taylor expansion

The equivalent single layer description requires an assumption of the displacement for the whole plate. Using Taylor expansions it can generally be written as

$$\boldsymbol{u} = z^r \boldsymbol{u}_r \quad r = 0, 1, 2, \ldots, N \tag{10}$$

Expressed in the form of the generalized assumption (9), the subscript b denotes values related to the reference surface Ω and the subscript t refers to the terms with the highest order (N). The thickness functions thus are the following Taylor expansions

$$F_b = 1, \quad F_t = z^N, \quad F_r = z^r, \quad r = 1, 2, \ldots, N - 1 \tag{11}$$

In this work we consider linear ($N = 1$) up to fourth-order ($N = 4$) models. These models are denoted as EDN where N indicates the order of expansion. For instance, for ED1 the explicit displacement assumptions read

$$u_x = u_{xb} + zu_{xt}$$
$$u_y = u_{yb} + zu_{yt}$$
$$u_z = u_{zb} + zu_{zt}$$

The variable u_{ib} represents the displacement of the reference surface Ω and the variable u_{it} is interpreted as the rotation angle ϕ_i. In this respect, the First order Shear Deformation Theory (FSDT) can be found by setting $u_{zt} = \phi_z = 0$. Furthermore, results for the Classical Laminate Theory (CLT) with the condition $u_{xt} = \phi_x = -u_{z,x}$ and $u_{yt} = \phi_y = -u_{z,y}$ can be obtained by using the shear correction factor $\chi = \infty$ within a typical penalty technique.

3.1.2. Inclusion of ZZ-functions in ESLM

A refinement of the ESL formulation can be reached by adding a function to the displacement assumption, that imposes the zig-zag form (ZZ) of the displacement distribution. According to Murakami [20], who first presented this idea, the displacement with imposed ZZ form reads

$$\boldsymbol{u} = \boldsymbol{u}_0 + (-1)^k \zeta_k \boldsymbol{u}_Z + z^r \boldsymbol{u}_r, \quad r = 1, 2, \ldots, N \quad (12)$$

The zig-zag term, denoted with the subscript Z changes sign for each layer k. In unified form this relation can be represented, if the subscript t is referred to the ZZ function ($\boldsymbol{u}_t = \boldsymbol{u}_Z$). In this case, the thickness functions are defined as

$$F_b = 1, \quad F_t = (-1)^k \zeta_k, \quad F_r = z^r, \quad r = 1, 2, \ldots, N \quad (13)$$

These ESLM with ZZ functions are considered with linear, parabolic and cubic expansion, referred to as EDZ1, EDZ2 and EDZ3. For example the explicit displacement assumptions of EDZ1 take the form

$$u_x = u_{x0} + z\phi_x + (-1)^k \zeta_k u_{xZ}$$
$$u_y = u_{y0} + z\phi_y + (-1)^k \zeta_k u_{yZ}$$
$$u_z = u_{z0} + z\phi_z + (-1)^k \zeta_k u_{zZ}$$

The construction of EDZ1 is depicted in Fig. 3.

3.1.3. LW model with Legendre expansions

In case of layer-wise modeling, the displacement variables are assumed independently for each layer k. Thus a statement in the unified form
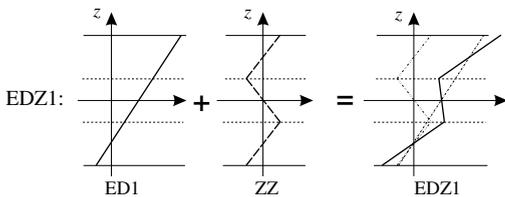
Fig. 3. Displacement assumptions of EDZ1.

$$\boldsymbol{u}^k = F_t \boldsymbol{u}_t^k + F_b \boldsymbol{u}_b^k + F_r \boldsymbol{u}_r^k = F_\tau \boldsymbol{u}_\tau^k$$

where $\tau = t, b, r$; $\quad r = 1, 2, \ldots, N$ and

$$k = 1, 2, \ldots, N_L \quad (14)$$

exists for every layer k. For LW models it is much more convenient to use combinations of Legendre polynomials as thickness functions. As they offer the possibility to define $\boldsymbol{u}_t$ and $\boldsymbol{u}_b$ as top and bottom values of the displacements of the layer, the interlaminar continuity can easily be implemented in the assembly of the laminate. The thickness functions F_τ for the LW case are defined as

$$F_b = (P_0 + P_1)/2, \quad F_t = (P_0 - P_1)/2,$$
$$F_r = P_r - P_{r-2} \quad \text{with } r = 1, 2, \ldots, N \quad (15)$$

in which $P_j = P_j(\zeta_k)$ is the Legendre polynomial of jth order defined over the layer thickness ζ_k with $-1 \leqslant \zeta_k \leqslant 1$. The LW models range as well from linear up to fourth-order (LD1, LD2, LD3 and LD4). The employed polynomials are in the following explicitly given:

$$P_0 = 1, \quad P_1 = \zeta_k, \quad P_2 = (3\zeta_k^2 - 1)/2,$$
$$P_3 = (5\zeta_k^3 - 3\zeta_k)/2, \quad P_4 = (35\zeta_k^4 - 30\zeta_k^2 + 3)/8$$

As the top and bottom values of the displacements have been chosen as unknown variables, the interlaminar compatibility can be imposed by

$$\boldsymbol{u}_t^k = \boldsymbol{u}_b^{(k+1)}, \quad k = 1, \ldots, N_L - 1 \quad (16)$$

3.2. Assumptions for potential

The modeling of the potential Φ will be restricted to layer-wise formulation. As hybrid problems containing piezoelectric and pure elastic layers are considered, the differences of the electric properties of each layer can be very significant. ESL assumptions thus do not seem appropriate to cover these high gradients. In contrast to the displacement $\boldsymbol{u}$, the potential Φ is a scalar. To obtain typical 3×3 matrices for the fundamental nuclei, it is useful for computational reasons that will be clarified later, to introduce the potential as a vector $\boldsymbol{\Phi}^k = [\Phi^k, \Phi^k, \Phi^k]^T$. Each component has the same value, the scalar potential Φ. With this assumption the layer-wise assumptions for the potential can be written in accordance to Eq. (14) as

$$\boldsymbol{\Phi}^k = F_t \boldsymbol{\Phi}_t^k + F_b \boldsymbol{\Phi}_b^k + F_r \boldsymbol{\Phi}_r^k = F_\tau \boldsymbol{\Phi}_\tau^k$$

where $\tau = t, b, r$; $\quad r = 1, 2, \ldots, N$

and $\quad k = 1, 2, \ldots, N_L \quad (17)$

The same thickness functions are used as in the layer-wise displacement case, stated in Eq. (15). The interlaminar compatibility conditions of the potential can thus be imposed by

$$\mathbf{\Phi}_t^k = \mathbf{\Phi}_b^{(k+1)}, \quad k = 1, \dots, N_L - 1 \tag{18}$$

For convenience the expansion N of the potential is assumed to be the same as the expansion of the displacement assumption, no matter if the latter is chosen to be ESL or LW.

4. Governing equations

The unified formulation of the differential equations and boundary conditions governing the coupled mechanical–electrical behavior of hybrid piezoelectric mechanic plates are derived in this section, using the principle of virtual displacements (PVD). The derivation is performed at layer-level, followed by the assembly of the arrays for the laminate. In the third part a Navier-type closed-form solution is presented.

4.1. Governing equations for a single layer

The PVD for a piezoelectric layer k in array formulation can be stated as

$$\int_{\Omega_k} \int_{A_k} \left\{ \delta \boldsymbol{\epsilon}_p^{k\mathrm{T}} \boldsymbol{\sigma}_p^k + \delta \boldsymbol{\epsilon}_n^{k\mathrm{T}} \boldsymbol{\sigma}_n^k - \delta \boldsymbol{E}^\mathrm{T} \widetilde{\boldsymbol{D}} \right\} \mathrm{d}\Omega_k \, \mathrm{d}z$$
$$= - \int_{\Omega_k} \int_{A_k} \rho_k \delta \boldsymbol{u}^{k\mathrm{T}} \ddot{\boldsymbol{u}}^k \mathrm{d}\Omega_k \, \mathrm{d}z + \delta W^e \tag{19}$$

The external virtual work is represented as δW^e. The geometrical relations (7) and (8) and the constitutive equations (6) are introduced and displacement and potential are expressed with the assumptions (9) and (17).

$$\int_{\Omega_k} \int_{A_k} \left\{ (\boldsymbol{D}_p \delta \boldsymbol{u}_\tau^k)^\mathrm{T} F_\tau \left[\left(\widetilde{\boldsymbol{C}}_{pp}^k \boldsymbol{D}_p + \widetilde{\boldsymbol{C}}_{pn}^k \boldsymbol{D}_n \right) F_s \boldsymbol{u}_s^k - \boldsymbol{e}_p^{k\mathrm{T}} \boldsymbol{D}_e F_s \mathbf{\Phi}_s^k \right] \right.$$
$$+ (\boldsymbol{D}_n \delta \boldsymbol{u}_\tau^k)^\mathrm{T} F_\tau \left[\left(\widetilde{\boldsymbol{C}}_{np}^k \boldsymbol{D}_p + \widetilde{\boldsymbol{C}}_{nn}^k \boldsymbol{D}_n \right) F_s \boldsymbol{u}_s^k - \boldsymbol{e}_n^{k\mathrm{T}} \boldsymbol{D}_e F_s \mathbf{\Phi}_s^k \right]$$
$$\left. - (\boldsymbol{D}_e \delta \mathbf{\Phi}_\tau^k)^\mathrm{T} F_\tau \left[\left(\boldsymbol{e}_p^k \boldsymbol{D}_p + \boldsymbol{e}_n^k \boldsymbol{D}_n \right) F_s \boldsymbol{u}_s^k + \boldsymbol{\varepsilon}^k \boldsymbol{D}_e F_s \mathbf{\Phi}_s^k \right] \right\} \mathrm{d}\Omega_k \, \mathrm{d}z$$
$$= - \int_{\Omega_k} \int_{A_k} \delta \boldsymbol{u}_\tau^{k\mathrm{T}} F_\tau \rho_k F_s \ddot{\boldsymbol{u}}_s^k \mathrm{d}\Omega_k \, \mathrm{d}z + \delta W_e \tag{20}$$

$\boldsymbol{D}_n$ and $\boldsymbol{D}_e$ contain the differential operators in both the in-plane and the transverse direction. In order to perform integration-by-parts in the domain Ω_k, these operators are conveniently splitted into their in-plane (subscript Ω) and transverse (subscript z) components:

$$\boldsymbol{D}_n = \boldsymbol{D}_{n\Omega} + \boldsymbol{D}_{nz} \tag{21}$$

$$\boldsymbol{D}_e = \boldsymbol{D}_{e\Omega} + \boldsymbol{D}_{ez} \tag{22}$$

The integration-by-parts in Ω_k can be carried out according to the following array scheme:

$$\int_{\Omega_k} (\boldsymbol{D}_\xi \delta \boldsymbol{u}^k)^\mathrm{T} \boldsymbol{u}^k \, \mathrm{d}\Omega_k = - \int_{\Omega_k} \delta \boldsymbol{u}^{k\mathrm{T}} \boldsymbol{D}_\xi^\mathrm{T} \boldsymbol{u}^k \, \mathrm{d}\Omega_k$$
$$+ \int_{\Gamma_k} \delta \boldsymbol{u}^{k\mathrm{T}} \boldsymbol{I}_\xi \boldsymbol{u}^k \, \mathrm{d}\Gamma_k$$

where $\xi = p, n\Omega, e\Omega$ \hfill (23)

with

$$\boldsymbol{I}_p = \begin{bmatrix} 1 & 0 & 0 \\ 0 & 1 & 0 \\ 1 & 1 & 0 \end{bmatrix}, \quad \boldsymbol{I}_{n\Omega} = \begin{bmatrix} 0 & 0 & 1 \\ 0 & 0 & 1 \\ 0 & 0 & 0 \end{bmatrix}$$

and

$$\boldsymbol{I}_{e\Omega} = \begin{bmatrix} -1 & 0 & 0 \\ 0 & -1 & 0 \\ 0 & 0 & 0 \end{bmatrix} \tag{24}$$

The integration yields following expression

$$\int_{\Omega_k} \int_{A_k} \left\{ \delta \boldsymbol{u}_\tau^{k\mathrm{T}} \left[-\boldsymbol{D}_p^\mathrm{T} F_\tau \left((\widetilde{\boldsymbol{C}}_{pp}^k \boldsymbol{D}_p + \widetilde{\boldsymbol{C}}_{pn}^k (\boldsymbol{D}_{n\Omega} + \boldsymbol{D}_{nz})) F_s \boldsymbol{u}_s^k \right. \right. \right.$$
$$\left. - \boldsymbol{e}_p^{k\mathrm{T}} (\boldsymbol{D}_{e\Omega} + \boldsymbol{D}_{ez}) F_s \mathbf{\Phi}_s^k \right)$$
$$+ (\boldsymbol{D}_{nz}^\mathrm{T} - \boldsymbol{D}_{n\Omega}^\mathrm{T}) F_\tau \left((\widetilde{\boldsymbol{C}}_{np}^k \boldsymbol{D}_p + \widetilde{\boldsymbol{C}}_{nn}^k (\boldsymbol{D}_{n\Omega} + \boldsymbol{D}_{nz})) F_s \boldsymbol{u}_s^k \right.$$
$$\left. \left. - \boldsymbol{e}_n^{k\mathrm{T}} (\boldsymbol{D}_{e\Omega} + \boldsymbol{D}_{ez}) F_s \mathbf{\Phi}_s^k \right) \right]$$
$$- \delta \mathbf{\Phi}_\tau^{k\mathrm{T}} \left[(\boldsymbol{D}_{ez}^\mathrm{T} - \boldsymbol{D}_{e\Omega}^\mathrm{T}) F_\tau \left((\boldsymbol{e}_p^k \boldsymbol{D}_p + \boldsymbol{e}_n^k (\boldsymbol{D}_{n\Omega} + \boldsymbol{D}_{nz})) F_s \boldsymbol{u}_s^k \right. \right.$$
$$\left. \left. + \boldsymbol{\varepsilon}^k (\boldsymbol{D}_{e\Omega} + \boldsymbol{D}_{ez}) F_s \mathbf{\Phi}_s^k \right) \right] \right\} \mathrm{d}\Omega_k \, \mathrm{d}z$$
$$+ \int_{\Gamma_k} \int_{A_k} \left\{ \delta \boldsymbol{u}_\tau^{k\mathrm{T}} \left[\boldsymbol{I}_p^\mathrm{T} F_\tau \left((\widetilde{\boldsymbol{C}}_{pp}^k \boldsymbol{D}_p + \widetilde{\boldsymbol{C}}_{pn}^k (\boldsymbol{D}_{n\Omega} + \boldsymbol{D}_{nz})) F_s \boldsymbol{u}_s^k \right. \right. \right.$$
$$\left. - \boldsymbol{e}_p^{k\mathrm{T}} (\boldsymbol{D}_{e\Omega} + \boldsymbol{D}_{ez}) F_s \mathbf{\Phi}_s^k \right)$$
$$+ \boldsymbol{I}_{n\Omega}^\mathrm{T} F_\tau \left((\widetilde{\boldsymbol{C}}_{np}^k \boldsymbol{D}_p + \widetilde{\boldsymbol{C}}_{nn}^k (\boldsymbol{D}_{n\Omega} + \boldsymbol{D}_{nz})) F_s \boldsymbol{u}_s^k \right.$$
$$\left. \left. - \boldsymbol{e}_n^{k\mathrm{T}} (\boldsymbol{D}_{e\Omega} + \boldsymbol{D}_{ez}) F_s \mathbf{\Phi}_s^k \right) \right]$$
$$- \delta \mathbf{\Phi}_\tau^{k\mathrm{T}} \left[\boldsymbol{I}_{e\Omega}^\mathrm{T} F_\tau ((\boldsymbol{e}_p^k \boldsymbol{D}_p + \boldsymbol{e}_n^k (\boldsymbol{D}_{n\Omega} + \boldsymbol{D}_{nz})) F_s \boldsymbol{u}_s^k \right.$$
$$\left. + \boldsymbol{\varepsilon}^k (\boldsymbol{D}_{e\Omega} + \boldsymbol{D}_{ez}) F_s \mathbf{\Phi}_s^k) \right] \right\} \mathrm{d}\Gamma_k \, \mathrm{d}z$$
$$= - \int_{\Omega_k} \int_{A_k} \delta \boldsymbol{u}_\tau^{k\mathrm{T}} F_\tau \rho_k F_s \ddot{\boldsymbol{u}}_s^k \mathrm{d}\Omega_k \, \mathrm{d}z + \delta W_e \tag{25}$$

From this equation, the coupled electro-mechanical system of governing equations can be obtained. The variations of displacement $\delta \boldsymbol{u}^k$ and potential $\delta \mathbf{\Phi}^k$ are independent and can be therefore formulated in two separate equations

$$\delta \boldsymbol{u}_\tau^k : \quad \boldsymbol{K}_{uu}^{k\tau s} \boldsymbol{u}_s^k + \boldsymbol{K}_{ue}^{k\tau s} \mathbf{\Phi}_s^k = -\boldsymbol{M}^{k\tau s} \ddot{\boldsymbol{u}}_s^k + \boldsymbol{p}_{m\tau}^k \tag{26}$$

$$\delta \mathbf{\Phi}_\tau^k : \quad \boldsymbol{K}_{eu}^{k\tau s} \boldsymbol{u}_s^k + \boldsymbol{K}_{ee}^{k\tau s} \mathbf{\Phi}_s^k = \boldsymbol{p}_{e\tau}^k \tag{27}$$

with the boundary conditions

$$\boldsymbol{u}_\tau^k = \bar{\boldsymbol{u}}_\tau^k \quad \text{or} \quad \boldsymbol{\Pi}_{uu}^{k\tau s} \boldsymbol{u}_s^k + \boldsymbol{\Pi}_{ue}^{k\tau s} \mathbf{\Phi}_s^k = \boldsymbol{\Pi}_{uu}^{k\tau s} \bar{\boldsymbol{u}}_s^k + \boldsymbol{\Pi}_{ue}^{k\tau s} \bar{\mathbf{\Phi}}_s^k$$
$$\mathbf{\Phi}_\tau^k = \bar{\mathbf{\Phi}}_\tau^k \quad \text{or} \quad \boldsymbol{\Pi}_{eu}^{k\tau s} \boldsymbol{u}_s^k + \boldsymbol{\Pi}_{ee}^{k\tau s} \mathbf{\Phi}_s^k = \boldsymbol{\Pi}_{eu}^{k\tau s} \bar{\boldsymbol{u}}_s^k + \boldsymbol{\Pi}_{ee}^{k\tau s} \bar{\mathbf{\Phi}}_s^k$$
$$\tag{28}$$

The unified formulation introduces the following fundamental nuclei

$$
\begin{aligned}
\boldsymbol{K}_{uu}^{k\tau s} = \int_{A_k} \Big\{ & -\boldsymbol{D}_p^{\mathrm{T}}\Big(\boldsymbol{C}_{pp}^k F_\tau F_s \boldsymbol{D}_p + \boldsymbol{C}_{pn}^k F_\tau F_s \boldsymbol{D}_{n\Omega} + \boldsymbol{C}_{pn}^k F_\tau \boldsymbol{D}_{nz}F_s \Big) \\
& -\boldsymbol{D}_{n\Omega}^{\mathrm{T}}\Big(\boldsymbol{C}_{np}^k F_\tau F_s \boldsymbol{D}_p + \boldsymbol{C}_{nn}^k F_\tau F_s \boldsymbol{D}_{n\Omega} + \boldsymbol{C}_{nn}^k F_\tau \boldsymbol{D}_{nz}F_s \Big) \\
& +\boldsymbol{D}_{nz}^{\mathrm{T}} F_\tau \Big(\boldsymbol{C}_{np}^k F_s \boldsymbol{D}_p + \boldsymbol{C}_{nn}^k F_s \boldsymbol{D}_{n\Omega} + \boldsymbol{C}_{nn}^k \boldsymbol{D}_{nz}F_s \Big) \Big\} \mathrm{d}z
\end{aligned}
\tag{29}
$$

$$
\begin{aligned}
\boldsymbol{K}_{ue}^{k\tau s} = \int_{A_k} \Big\{ & \boldsymbol{D}_p^{\mathrm{T}}\Big(\boldsymbol{e}_p^{k\mathrm{T}} F_\tau \boldsymbol{D}_{ez}F_s + \boldsymbol{e}_p^{k\mathrm{T}} F_\tau F_s \boldsymbol{D}_{e\Omega} \Big) \\
& +\boldsymbol{D}_{n\Omega}^{\mathrm{T}}\Big(\boldsymbol{e}_n^{k\mathrm{T}} F_\tau \boldsymbol{D}_{ez}F_s + \boldsymbol{e}_n^{k\mathrm{T}} F_\tau F_s \boldsymbol{D}_{e\Omega} \Big) \\
& -\boldsymbol{D}_{nz}^{\mathrm{T}} F_\tau \Big(\boldsymbol{e}_n^{k\mathrm{T}} \boldsymbol{D}_{ez}F_s + \boldsymbol{e}_n^{k\mathrm{T}} F_s \boldsymbol{D}_{e\Omega} \Big) \Big\} \mathrm{d}z
\end{aligned}
\tag{30}
$$

$$
\begin{aligned}
\boldsymbol{K}_{eu}^{k\tau s} = \int_{A_k} \Big\{ & \boldsymbol{D}_{e\Omega}^{\mathrm{T}}\Big(\boldsymbol{e}_p^k F_\tau F_s \boldsymbol{D}_p + \boldsymbol{e}_n^k F_\tau \boldsymbol{D}_{nz}F_s + \boldsymbol{e}_n^k F_\tau F_s \boldsymbol{D}_{n\Omega} \Big) \\
& -\boldsymbol{D}_{ez}^{\mathrm{T}} F_\tau \Big(\boldsymbol{e}_p^k F_s \boldsymbol{D}_p + \boldsymbol{e}_n^k \boldsymbol{D}_{nz}F_s + \boldsymbol{e}_n^k F_s \boldsymbol{D}_{n\Omega} \Big) \Big\} \mathrm{d}z
\end{aligned}
\tag{31}
$$

$$
\begin{aligned}
\boldsymbol{K}_{ee}^{k\tau s} = \int_{A_k} \Big\{ & \boldsymbol{D}_{e\Omega}^{\mathrm{T}}\big(\boldsymbol{\varepsilon}^k F_\tau \boldsymbol{D}_{ez}F_s + \boldsymbol{\varepsilon}^k F_\tau F_s \boldsymbol{D}_{e\Omega} \big) \\
& -\boldsymbol{D}_{ez}^{\mathrm{T}} F_\tau \big(\boldsymbol{\varepsilon}^k \boldsymbol{D}_{ez}F_s + \boldsymbol{\varepsilon}^k F_s \boldsymbol{D}_{e\Omega} \big) \Big\} \mathrm{d}z
\end{aligned}
\tag{32}
$$

The matrices for the boundary terms read

$$
\begin{aligned}
\boldsymbol{\Pi}_{uu}^{k\tau s} = \int_{A_k} \Big\{ & \boldsymbol{I}_p(\boldsymbol{C}_{pp}^k F_\tau F_s \boldsymbol{D}_p + \boldsymbol{C}_{pn}^k F_\tau F_s \boldsymbol{D}_{n\Omega} + \boldsymbol{C}_{pn}^k F_\tau \boldsymbol{D}_{nz}F_s) \\
& +\boldsymbol{I}_{n\Omega}(\boldsymbol{C}_{np}^k F_\tau F_s \boldsymbol{D}_p + \boldsymbol{C}_{nn}^k F_\tau F_s \boldsymbol{D}_{n\Omega} + \boldsymbol{C}_{nn}^k F_\tau \boldsymbol{D}_{nz}F_s) \Big\} \mathrm{d}z
\end{aligned}
\tag{33}
$$

$$
\begin{aligned}
\boldsymbol{\Pi}_{ue}^{k\tau s} = \int_{A_k} \Big\{ & -\boldsymbol{I}_p\Big(\boldsymbol{e}_p^{k\mathrm{T}} F_\tau \boldsymbol{D}_{ez}F_s + \boldsymbol{e}_p^{k\mathrm{T}} F_\tau F_s \boldsymbol{D}_{e\Omega} \Big) \\
& -\boldsymbol{I}_{n\Omega}\Big(\boldsymbol{e}_n^{k\mathrm{T}} F_\tau \boldsymbol{D}_{ez}F_s + \boldsymbol{e}_n^{k\mathrm{T}} F_\tau F_s \boldsymbol{D}_{e\Omega} \Big) \Big\} \mathrm{d}z
\end{aligned}
\tag{34}
$$

$$
\boldsymbol{\Pi}_{eu}^{k\tau s} = \int_{A_k} -\Big\{ \boldsymbol{I}_{e\Omega}^{\mathrm{T}}\Big(\boldsymbol{e}_p^k F_\tau F_s \boldsymbol{D}_p + \boldsymbol{e}_n^k F_\tau \boldsymbol{D}_{nz}F_s + \boldsymbol{e}_n^k F_\tau F_s \boldsymbol{D}_{n\Omega} \Big) \Big\} \mathrm{d}z
\tag{35}
$$

$$
\boldsymbol{\Pi}_{ee}^{k\tau s} = \int_{A_k} -\Big\{ \boldsymbol{I}_{e\Omega}^{\mathrm{T}}\big(\boldsymbol{\varepsilon}^k F_\tau \boldsymbol{D}_{ez}F_s + \boldsymbol{\varepsilon}^k F_\tau F_s \boldsymbol{D}_{e\Omega} \big) \Big\} \mathrm{d}z
\tag{36}
$$

and the mass matrix can be calculated as

$$
\boldsymbol{M}^{k\tau s} = \int_{A_k} \{ \rho^k F_\tau F_s \boldsymbol{I} \} \mathrm{d}z
\tag{37}
$$

The explicit form of the fundamental nuclei for monoclinic material properties is stated in Appendix A.1.

4.2. Assembly of laminate arrays

In the previous section the fundamental matrices for piezoelectric layers have been derived. They are build
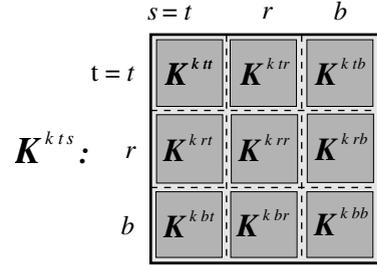
Fig. 4. Basic scheme of layer arrays $\boldsymbol{K}_{ij}^{k\tau s}$ ($i,j = u,e$).

according to the scheme displayed in Fig. 4, where the indices τ and s give the positions t, r and b as defined for the generalized assumptions. In case of displacements, each subpart tt, tr etc. consist of the three components u_x, u_y and u_z. The scalar electric potential has been artificially expanded to a $[3 \times 1]$ vector, thus leading to a $[3 \times 3]$ fundamental nucleus analogous to the displacements. During assembly, the terms related to the potential can be contracted back to their scalar nature. While $\boldsymbol{K}_{uu}^{k\tau s}$ has the dimension $[3 \times 3]$, $\boldsymbol{K}_{ue}^{k\tau s}$ and $\boldsymbol{K}_{eu}^{k\tau s}$ become $[3 \times 1]$ and $[1 \times 3]$ arrays, respectively, and $\boldsymbol{K}_{ee}^{k\tau s}$ is reduced to a $[1 \times 1]$ matrix.

4.2.1. LW assembly

If the displacement is assumed layer-wise, the layer arrays $\boldsymbol{K}_{ij}^{k\tau s}$ with $(ij) = (uu)$, (ue), (eu) and (ee), are combined to the laminate matrices $\boldsymbol{K}_{ij}^{\tau s}$ according to the scheme in Fig. 5. The interface conditions for the displacements and the potential Eqs. (16) and (18) are imposed by superposing the related subparts as demonstrated in the figure.

4.2.2. ESL assembly

In case of ESL modeling only one set of displacements $\boldsymbol{u}$ exists. Thus the layer arrays $\boldsymbol{K}_{uu}^{k\tau s}$ are all superposed on this displacement. The potential is still modeled LW, so that for $\boldsymbol{K}_{ue}^{k\tau s}$ and $\boldsymbol{K}_{eu}^{k\tau s}$ only the displacements and the top and bottom potentials at each layer
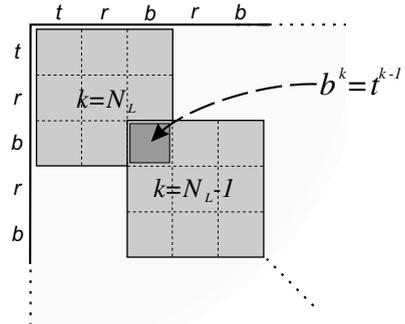
Fig. 5. LW assembly of laminate arrays $\boldsymbol{K}_{ij}^{\tau s}$ ($i,j = u,e$).
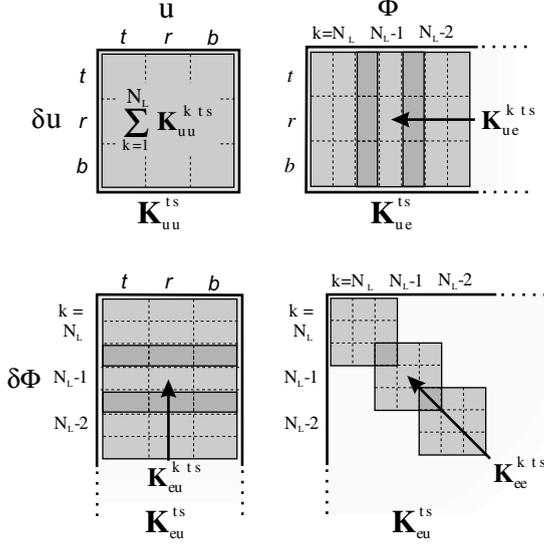
Fig. 6. ESL assembly of laminate arrays $\boldsymbol{K}_{ij}^{\tau s}$ $(i,j = u,e)$.

interface are superposed. At last $K_{ee}^{k\tau s}$ is assembled as in the pure LW case. This assembly procedure is depicted in Fig. 6.

4.3. Closed-form solution

Closed-form solution to the problem given by Eqs. (26)–(28) can be found, if some restrictions are applied. The considered plate must be simply-supported which implies the following boundary conditions on the displacements:

$$
\begin{aligned}
u_x^k(x,y,z) &= 0 \quad \text{at } y = 0, b \\
u_y^k(x,y,z) &= 0 \quad \text{at } x = 0, a \\
u_z^k(x,y,z) &= 0 \quad \text{at } x = 0, a \quad y = 0, b
\end{aligned}
\tag{38}
$$

In addition each layer is orthotropic in the laminate reference system, i.e. the components $\widetilde{C}_{16}$, $\widetilde{C}_{26}$, $\widetilde{C}_{36}$ and $\widetilde{C}_{45}$ vanish. In this case, the following Navier-type assumptions can be made

$$
\begin{aligned}
\left(u_{x\tau}^k, p_{mx\tau}^k\right) &= \left(\hat{u}_{x\tau}^k, \hat{p}_{mx\tau}^k\right)\cos(\alpha x)\sin(\beta y)e^{i\omega_{mn}t} \\
\left(u_{y\tau}^k, p_{my\tau}^k\right) &= \left(\hat{u}_{y\tau}^k, \hat{p}_{my\tau}^k\right)\sin(\alpha x)\cos(\beta y)e^{i\omega_{mn}t} \\
\left(u_{z\tau}^k, p_{mz\tau}^k\right) &= \left(\hat{u}_{z\tau}^k, \hat{p}_{mz\tau}^k\right)\sin(\alpha x)\sin(\beta y)e^{i\omega_{mn}t}
\end{aligned}
\tag{39}
$$

and

$$
\left(\Phi_\tau^k, p_{e\tau}^k\right) = \left(\hat{\Phi}_\tau^k, \hat{p}_{e\tau}^k\right)\sin(\alpha x)\sin(\beta y)e^{i\omega_{mn}t}
\tag{40}
$$

with the abbreviations

$$
\alpha = \frac{m\pi}{a} \quad \text{and} \quad \beta = \frac{n\pi}{b}
\tag{41}
$$

The factors m and n are the number of waves in x- and y-direction while a and b are the length and width of the

plate. Introducing these assumptions in the system of governing equations and carrying out the differentiations, the fundamental nuclei for closed-form solution $\hat{\boldsymbol{K}}_{uu}^{k\tau s}$, $\hat{\boldsymbol{K}}_{ue}^{k\tau s}$, $\hat{\boldsymbol{K}}_{eu}^{k\tau s}$ and $\hat{\boldsymbol{K}}_{ee}^{k\tau s}$ can be found. It turns out that $\hat{\boldsymbol{K}}_{eu}^{k\tau s} = \hat{\boldsymbol{K}}_{ue}^{k\tau s^{\mathrm{T}}}$. Explicit forms of these arrays can be taken from Appendix A.2. The assembly of the laminate arrays works in the same manner as described above. Thus the linear system for closed-form solution states

$$
\hat{\boldsymbol{K}}_{uu}\hat{\boldsymbol{u}} + \hat{\boldsymbol{K}}_{ue}\hat{\boldsymbol{\Phi}} = \omega_{mn}^2\boldsymbol{M}\hat{\boldsymbol{u}} + \hat{\boldsymbol{p}}_m
\tag{42}
$$

$$
\hat{\boldsymbol{K}}_{ue}^{\mathrm{T}}\hat{\boldsymbol{u}} + \hat{\boldsymbol{K}}_{ee}\hat{\boldsymbol{\Phi}} = \hat{\boldsymbol{p}}_e
\tag{43}
$$

The dynamic free vibration frequencies of this problem can be found by solving the eigenvalue problem

$$
\left\| \hat{\boldsymbol{K}}_{uu} - \left(\hat{\boldsymbol{K}}_{ue}\left(\hat{\boldsymbol{K}}_{ee}\right)^{-1}\hat{\boldsymbol{K}}_{ue}^{\mathrm{T}}\right) - \omega_{mn}^2\boldsymbol{M} \right\| = 0
\tag{44}
$$

Static responses to mechanical and electrical loadings $\hat{\boldsymbol{p}}_m$ and $\hat{\boldsymbol{p}}_e$ can be calculated if the loadings are in the form of Eqs. (39) and (40). Boundary conditions on the potential $\hat{\boldsymbol{\Phi}}$ can be imposed on the top and bottom surface and at the layer interfaces; in all cases, $\hat{\boldsymbol{\Phi}}$ is continuous along z.

5. Numerical results

Three different problems have been addressed. The first is a dynamic analysis and the second and third consider the static response of a plate on two different loading and boundary condition configurations. For all three problems 3D exact solutions are available, which are used for the verification of the presented model.

5.1. Definition of problems

5.1.1. Problem I

In this testcase a square plate with the length and width a and the thickness h is considered, see Fig. 7. It consists of five layers which are assumed to be perfectly bonded to each other. The top and bottom layers are made of piezoelectric materials with the thickness
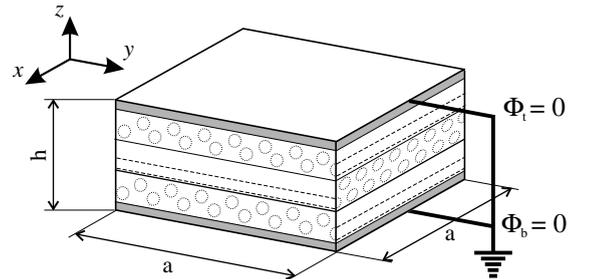
Fig. 7. Problem I, geometry and boundary conditions.

Table 1
Elastic, piezoelectric and dielectric properties of used materials

Property	PZT-4	Gr/EP
E_1 [GPa]	81.3	132.38
E_2 [GPa]	81.3	10.756
E_3 [GPa]	64.5	10.756
v_{12} [–]	0.329	0.24
v_{13} [–]	0.432	0.24
v_{23} [–]	0.432	0.49
G_{44} [GPa]	25.6	3.606
G_{55} [GPa]	25.6	5.6537
G_{66} [GPa]	30.6	5.6537
e_{15} [C/m^2]	12.72	0
e_{24} [C/m^2]	12.72	0
e_{31} [C/m^2]	−5.20	0
e_{32} [C/m^2]	−5.20	0
e_{33} [C/m^2]	15.08	0
$\bar{\epsilon}_{11}/\epsilon_0$ [–]	1475	3.5
$\bar{\epsilon}_{22}/\epsilon_0$ [–]	1475	3.0
$\bar{\epsilon}_{33}/\epsilon_0$ [–]	1300	3.0

Fig. 8. Problem II, geometry, boundary conditions and loading configuration.

$h_p^k = 0.1h$ each, the three structural layers of equal thickness have the configuration [0/90/0]. The materials are PZT-4 for the piezoelectric and Gr/Ep for the structural layers. The corresponding material properties can be taken from Table 1. The top and bottom surfaces are assumed to be traction-free and electrically grounded, which imposes the electric potential to be zero ($\Phi_t = \Phi_b = 0$). The free vibration frequencies for one wave in each direction ($m = n = 1$) are calculated in means of the frequency parameter $\gamma = \omega/100$. Four thickness ratios $a/h = 2$, 4, 10 and 50 are considered. A 3D exact solution is available from Heyliger and Saravanos [22] for the cases $a/h = 4$ and 50. Further numerical results for these cases can be taken from Benjeddou [15] and Touratier and Ossadzow-David [13].

5.1.2. Problem II

The configuration for Problem II and III consists of a simply supported square plate with the side length a and the thickness h. It is build of four layers, two layers of fiber reinforced material as a structural core on top and bottom of which the two piezoelectric layers are bonded. The core layers have the thickness $h_c = 0.4h$ each and the fiber direction is in [0/90] configuration.

The thickness of each piezoelectric layer is $h_p = 0.1h$. The materials are PZT-4 and Gr/Ep with the same properties as used for Problem I (Table 1). The analytic solution is calculated for one wave in each direction ($m = n = 1$). Four different thickness ratios $a/h = 2$, 4, 10 and 100 are considered.

For Problem II, a mechanical loading of $\hat{p}_z = 1$ is applied on the top surface of the plate. The top and bottom surfaces are electrically grounded and thus have the potential $\Phi_t = \Phi_b = 0$. The configuration of Problem II is shown in Fig. 8. 3D exact solution to Problems II and III for $a/h = 4$ were presented by Heyliger [23].

5.1.3. Problem III

The plate of Problem III is the same as for Problem II and again a closed-form solution is determined for $m = n = 1$. Only the boundary conditions and loading configurations are changed as shown in Fig. 9. The
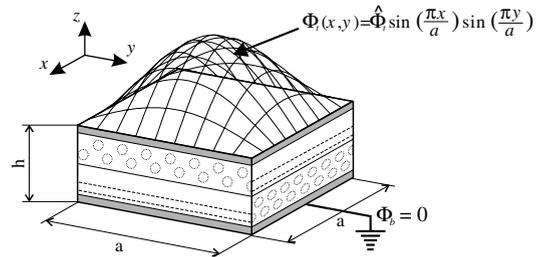
Fig. 9. Problem III, geometry, boundary conditions and loading configuration.

Table 2
Verification—Problem I, frequency parameters $\gamma = \omega/100$ of exact solution and LD4

a/h		Mode 1	Mode 2	Mode 3	Mode 4	Mode 5	Mode 6
4	Exact	57074.5	191301	250769	274941	362492	381036
	LD4	57074.0	191301	250768	274940	362489	381036
50	Exact	618.118	15681.6	21492.8	209704	210522	378104
	LD4	618.104	15681.6	21492.6	209704	210522	378104

Table 3
Verification—Problem II, thickness distribution of Φ, σ_{xx} and $\widetilde{D}$ of exact solution and LD4

z	$\Phi \times 10^3$		σ_{xx}		$\widetilde{D}$	
	Exact	LD4	Exact	LD4	Exact	LD4
0.500	0.0000	0.000	6.5643	6.5642	160.58	160.59
0.475	0.0189	0.189	5.8201	5.8200	149.35	149.35
0.450	0.0358	0.352	5.0855	5.0855	117.23	117.23
0.425	0.0488	0.488	4.3595	4.3595	66.568	66.567
0.400	0.0598	0.598	3.6408	3.6408	−0.3382	−0.3348
0.400	0.0598	0.598	2.8855	2.8858	−0.3382	−0.3384
0.300	0.0589	0.590	1.4499	1.4496	−0.1276	−0.1277
0.200	0.0589	0.589	0.2879	0.2880	0.0813	0.0813
0.100	0.0596	0.593	−0.7817	−0.7814	0.2913	0.2914
0.000	0.0611	0.611	−1.9266	−1.9266	0.5052	0.5053
0.000	0.0611	0.611	0.0991	0.0991	0.5052	0.5053
−0.100	0.0634	0.634	−0.0149	−0.0150	0.7259	0.7260
−0.200	0.0665	0.666	−0.1280	−0.1281	0.9563	0.9565
−0.300	0.0706	0.706	−0.2426	−0.2427	1.1995	1.1997
−0.400	0.0756	0.756	−0.3616	−0.3617	1.4587	1.4589
−0.400	0.0756	0.756	−4.2348	−4.2348	1.4587	1.4559
−0.425	0.0602	0.602	−4.8806	−4.8806	−58.352	−58.351
−0.450	0.0425	0.425	−5.5337	−5.5337	−103.66	−103.67
−0.475	0.0224	0.225	−6.1951	−6.1950	−132.40	−132.41
−0.500	0.0000	0.000	−6.8658	−6.8658	−142.46	−142.46

Table 4
Verification—Problem III, thickness distribution of u_x, σ_{xx} and Φ of exact solution and LD4

z	$u_x \times 10^{12}$		σ_{xx}		Φ	
	Exact	LD4	Exact	LD4	Exact	LD4
0.500	−32.764	−32.765	111.81	111.80	1.0000	1.0000
0.475	−23.349	−23.350	63.736	63.738	0.9971	0.9972
0.450	−13.973	−13.974	15.833	15.839	0.9950	0.9951
0.425	−4.6174	−4.6179	−32.001	−31.992	0.9936	0.9936
0.400	4.7356	4.7353	−79.865	−79.852	0.9929	0.9929
0.400	4.7356	4.7353	−51.681	−51.680	0.9929	0.9929
0.300	2.9808	2.9802	−33.135	−33.127	0.8415	0.8416
0.200	1.7346	1.7346	−19.840	−19.840	0.7014	0.7015
0.100	0.8008	0.8014	−9.7737	−9.7780	0.5707	0.5708
0.000	0.0295	0.0297	−1.3905	−1.3953	0.4476	0.4477
0.000	0.0295	0.0297	−1.3089	−1.3099	0.4476	0.4477
−0.100	−0.4404	−0.4401	−0.5782	−0.5778	0.3305	0.3306
−0.200	−0.8815	−0.8812	0.1348	0.1343	0.2179	0.2179
−0.300	−1.3206	−1.3202	0.8463	0.8465	0.1081	0.1082
−0.400	−1.7839	−1.7835	1.5723	1.5708	−0.0010	−0.0010
−0.400	−1.7839	−1.7835	14.529	14.524	−0.0010	−0.0010
−0.425	−2.0470	−2.0465	178.01	17.793	−0.0009	−0.0010
−0.450	−2.3140	−2.3134	210.98	21.090	−0.0008	−0.0008
−0.475	−2.5856	−2.5850	244.28	24.418	−0.0004	−0.0004
−0.500	−2.8625	−2.8618	277.95	27.784	0.0000	0.0000

top and bottom surfaces are now traction free and a potential of $\hat{\Phi}_t = 1$ is imposed on the top surface of the plate. The bottom surface remains grounded and thus has the potential $\Phi_b = 0$.

5.2. Verification

To verify the presented model and to assess its accuracy a comparison with results from the 3D exact
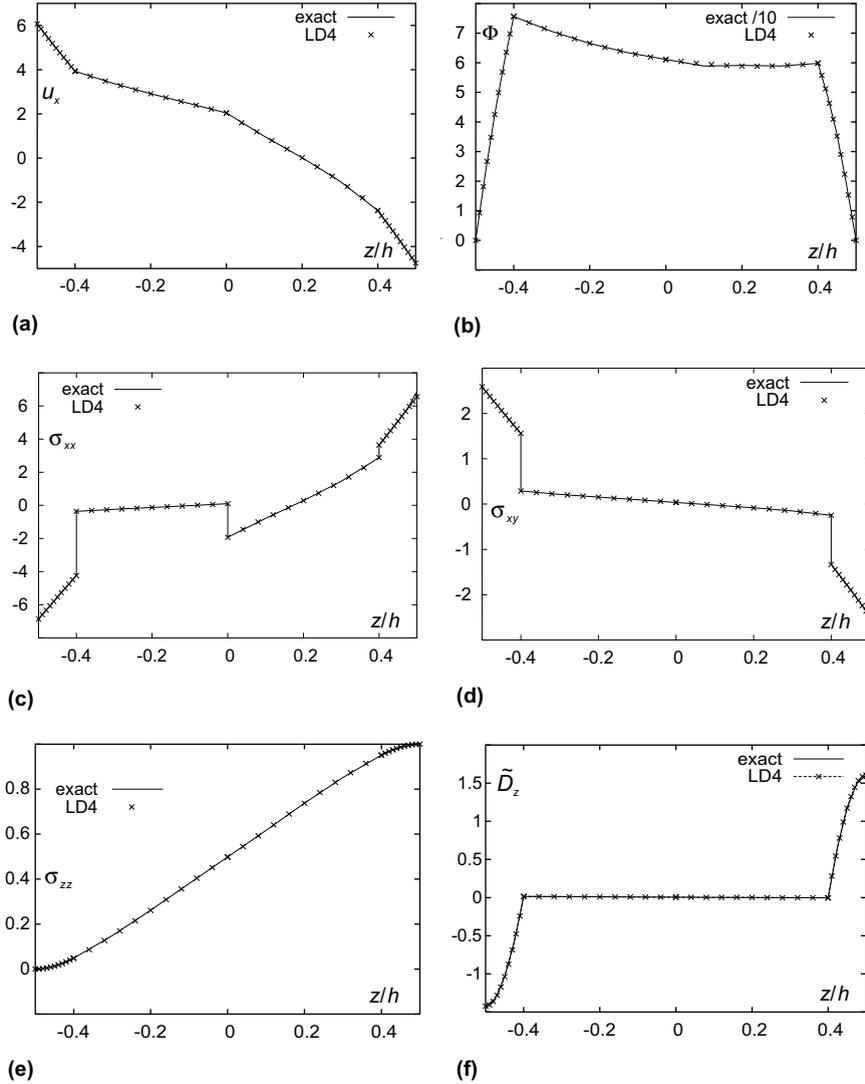
Fig. 10. Verification—Problem II, thickness distribution of selected variables: (a) displacement $u \times 10^{11}$, (b) potential $\Phi \times 10^3$, (c) in-plane stress σ_{xx}, (d) in-plane stress σ_{xy}, (e) normal stress σ_{zz}, (f) dielectric displacement $\tilde{D}_z \times 10^{11}$.

solution is presented. Attention is restricted to the LD4 plate theory which is supposed to lead to the best description (see also next section). The exact solution for Problem I taken from Heyliger and Saravanos [22] is available for the thickness ratios $a/h = 4$ and 50. Table 2 shows the results for the frequency parameter $\gamma = \omega / 100$ for the first six modes of the exact solution and LD4 model of the unified formulation. The differences between the two solutions is extremely small.

For Problems II and III the 3D exact solution for the thickness ratio $a/h = 4$ was calculated by Heyliger [23]. In Table 3 the results for the thickness distribution of the potential Φ, the in-plane stress σ_{xx} and the normal dielectric displacement $\tilde{D}_z$ of the exact solution and

LD4 are confronted. Table 4 contains the in-plane displacement u_x, the in-plane stress σ_{xx} and the potential Φ for Problem III. With two exceptions the results match with high accuracy. The first discrepancy occurs for the potential Φ in Table 3, where all results differ exactly with the factor ten. As all other results of Problem II depending partly on the potential are calculated consistently by the two models this discrepancy could not be more than a printing error. The second difference can be observed for the stresses σ_{xx} for Problem III (Table 4). Also here exactly factor ten occurs for the results in the bottom layer ($-0.5 \leqslant z \leqslant 0.4$). In the Figs. 10 and 11 the thickness distributions of some selected variables are printed together with the results from the exact
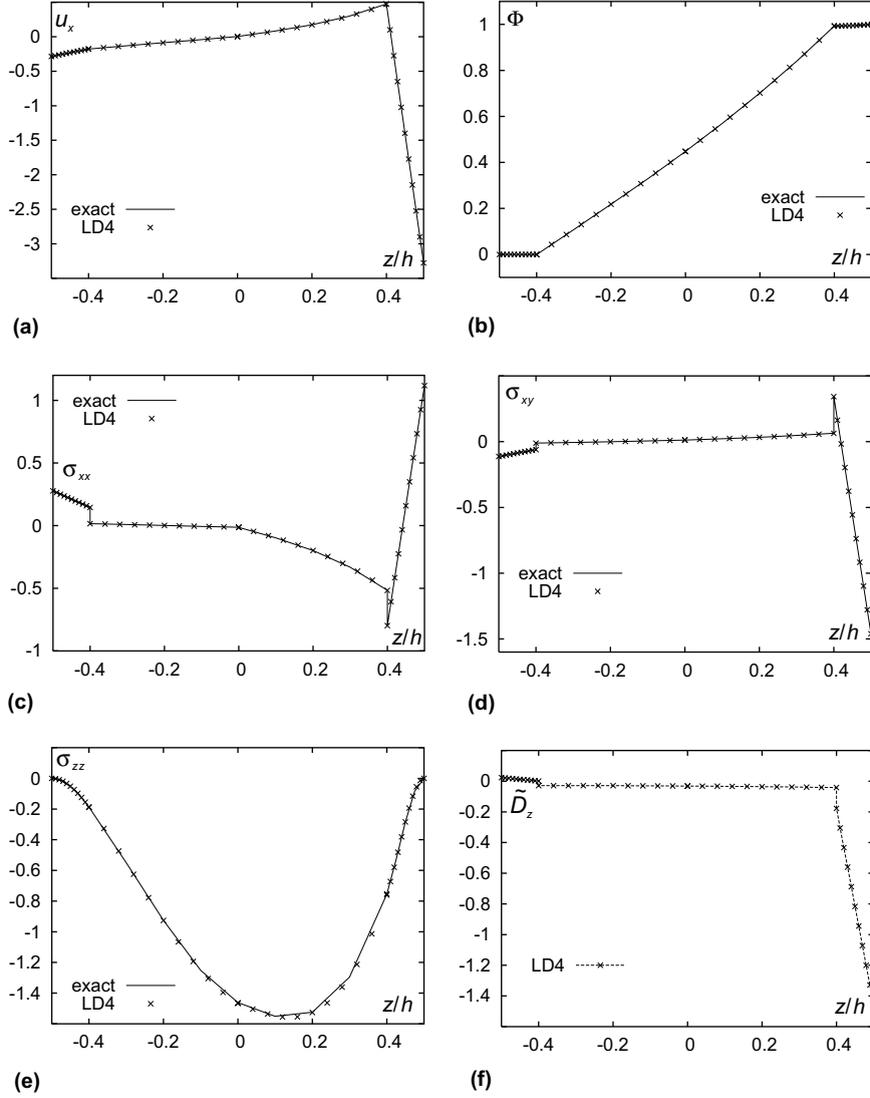
Fig. 11. Verification—Problem III, thickness distribution of selected variables: (a) displacement $u \times 10^{11}$, (b) potential Φ, (c) in-plane stress σ_{xx}, (d) in-plane stress σ_{xy}, (e) normal stress σ_{zz}, (f) dielectric displacement $\widetilde{D}_z \times 10^9$.

solution. In the two cases of discrepancies, the latter is corrected by the factor ten.

It can be concluded, that LD4 leads to a quasi-3D description of the dynamic and static response of multi-layered plates embedding piezoelectric layers. LD4 therefore could be used as reference solutions in those cases in which 3D solutions are not available.

5.3. Assessment of models

5.3.1. Problem I

Table 5 shows an overview of the frequency parameter results for all the considered theories for the thick-ness ratios $a/h = 4$ and 50, Table 6 for the ratios $a/h = 2$ and 10. In the first Table the results from the exact solution and the additional models of Benjeddou [12] and of Touratier and Ossadzow-David [13] are also listed. As expected the LDN models yield the best re-sults. The ESL models with imposed zig-zag form EDZN lead in the most cases to a slight improvement compared to the EDN models. The thickness distribu-tions related to the three first modes from LD4, ED4 and ED1 are plotted in Fig. 12 for the thickness ratio $a/h = 4$. Comparing the plots with the results in Table 5 it can be observed how a lower order of expansion leads to a decreasing accuracy of the description.

Table 5
Problem I, frequency parameters $\gamma = \omega/100$ for $a/h = 4$ and $a/h = 50$

	$a/h = 4$			$a/h = 50$		
	Mode 1	Mode 2	Mode 3	Mode 1	Mode 2	Mode 3
Exact	57074.5	191301	250769	618.118	15681.6	21492.8
Touratier	–	194903	251763	–	15592.3	–
Benjeddou	58216.1	196018	268650	618.435	15684.0	21499.4
LD4	57074.0	191301	250768	618.104	15681.6	21492.6
LD3	57074.0	191301	250768	618.104	15681.6	21492.6
LD2	57081.9	191311	250786	618.105	15681.6	21492.6
LD1	57252.5	194840	255646	619.022	15683.4	21494.4
ED4	58713.8	194592	254740	618.464	15693.5	21497.8
ED3	58818.6	195825	259586	618.550	15694.2	21500.1
ED2	69413.7	195860	261780	620.229	15694.9	21505.2
ED1	74105.9	196021	266337	689.867	15695.0	21507.4
EDZ3	57656.7	195711	259570	618.382	15687.1	21496.5
EDZ2	60605.5	195722	260861	619.046	15693.6	21496.5
EDZ1	63204.7	195965	266196	688.082	15693.6	21498.5
FSDT	74106.0	198465	286795	689.867	15877.2	22943.9
CLT	103031	198465	286795	692.254	15877.2	22943.9

Table 6
Problem I, frequency parameters $\gamma = \omega/100$ for $a/h = 2$ and $a/h = 10$

	$a/h = 2$			$a/h = 10$		
	Mode 1	Mode 2	Mode 3	Mode 1	Mode 2	Mode 3
LD4	136604	335749	366474	13526.4	78109.0	106609
LD3	136604	335756	366488	13526.4	78109.0	106609
LD2	136649	336016	366872	13526.8	78109.1	106609
LD1	137146	353823	393079	13559.0	78341.8	106852
ED4	143323	350268	390911	13655.1	78367.5	106834
ED3	144132	356910	398560	13660.0	78454.3	107125
ED2	179344	388934	482764	14446.5	78455.5	107125
ED1	186674	390737	510310	15886.5	78465.0	107395
EDZ3	138549	355557	398557	13584.0	78417.2	107113
EDZ2	146518	377442	416670	13858.1	78445.1	107118
EDZ1	148881	389638	443702	15080.1	78456.9	107372
FSDT	186674	396928	500510	15886.5	79386.2	114719
CLT	364185	396928	573563	17066.5	79386.2	114719

The two additional models lie in the range of the higher order ESL and the lower order LW models, depending on the thickness ratio and the mode.

5.3.1.1. *Influence of order of expansion.* In Table 7 the influence of the order of expansion N on the first mode of LDN and EDN models is summarized. For each model the number of degrees of freedom (NDOF) and the error to the exact solution (LD4) is given. For the LDN models an increase from $N = 2$ to 4 has nearly no effect, because even LD2 yields only marginal errors.

Thus the doubling of the NDOF from LD2 to LD4 is not very necessary. For the ED models in contrast, N is more relevant. The thick plate case requires at least third order and the thin plate case at least quadratic expansion to obtain good results. Comparing the higher order EDN with the lower order LDN models it can be noted, that for the given problem the latter yield better results although the implied NDOF is nearly the same.

5.3.1.2. *Influence of piezoelectric effect.* The influence of the piezoelectric coupling effects on the free vibration of
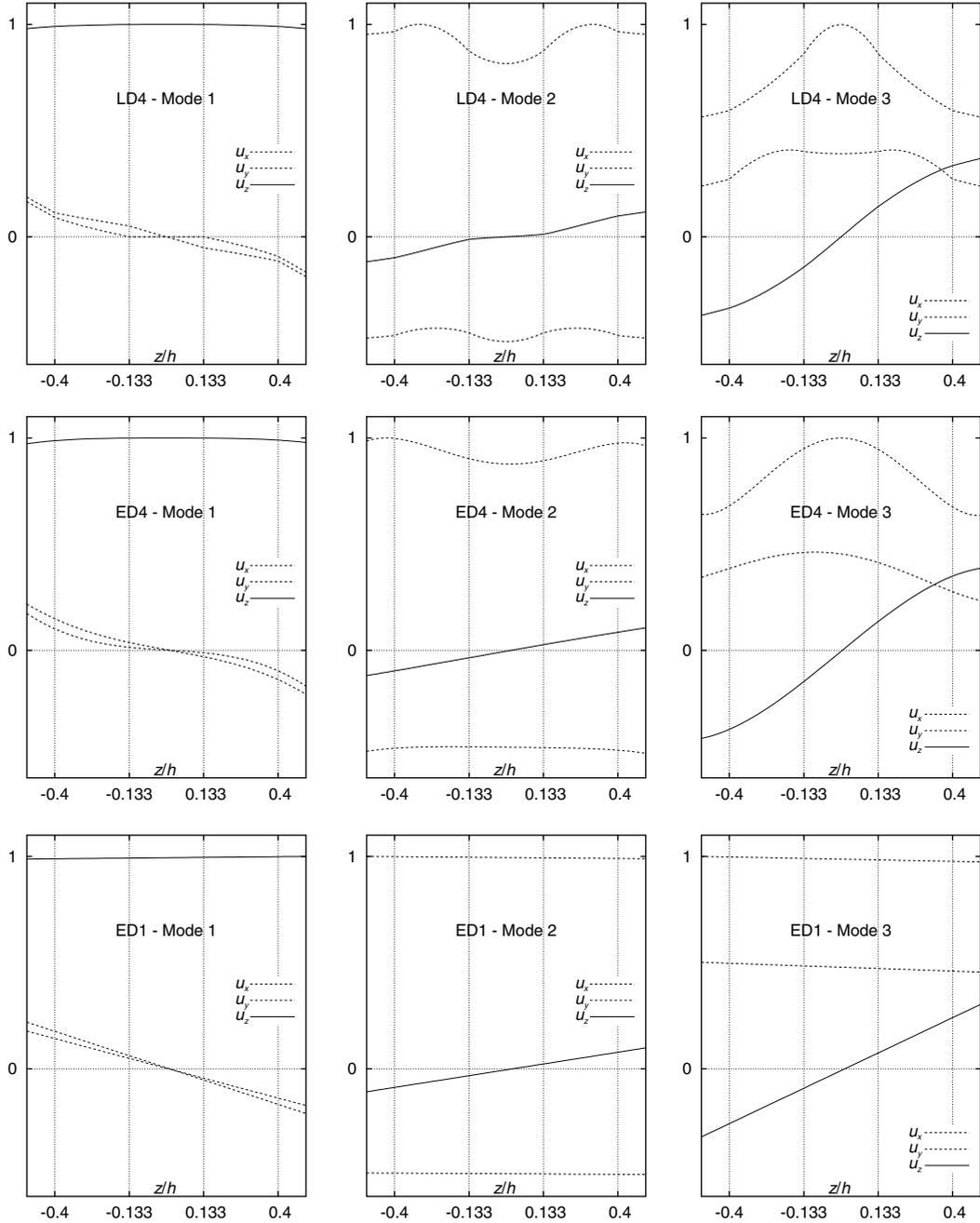
Fig. 12. Problem I, free vibration modes 1–3 of LD4, ED4 and ED1, $a/h = 4$.

the considered plate is examined in Table 8. The results are calculated with the presented LD4 model, for the mechanic case neglecting the piezoelectric coupling terms and thus considering only the elastic properties of the piezoelectric layers (LD4m). The coupling effect can be interpreted as an additional stiffness of the plate, which shows an increasing influence on the vibrational

behaviour with decreasing thickness of the considered plate.

5.3.2. Problem II—sensor configuration

Some selected results for the static calculation of Problem II are given in Table 9. The Problem II examines the response of a piezoelectric plate to a mechanical

Table 7
Problem I, influence of order of expansion N on first frequency parameter γ of LDN- and EDN-models

a/h	N	LDN			EDN		
		NDOF	γ_1	Δ [%]	NDOF	γ_1	Δ [%]
4	4	84	57074.0		36	58713.8	2.87
	3	64	57074.0	0.000	28	58818.6	3.06
	2	44	57081.9	0.014	20	69413.7	21.6
	1	24	57252.5	0.313	12	74105.9	29.84
50	4	84	618.104		36	618.464	0.06
	3	64	618.104	0.000	28	618.550	0.07
	2	44	618.105	0.000	20	620.229	0.34
	1	24	619.022	0.149	12	689.867	11.61

Table 8
Problem I, influence of piezoelectric effect on first frequency parameters γ_1

	a/h			
	2	4	10	50
LD4	136 604	57074.0	13526.4	618.104
LD4m	134 551	55514.8	12905.6	584.085
Δ [%]	1.50	2.73	4.59	5.50

Table 9
Problem II, selected results for w, σ_{xx}, σ_{xz}, Φ and $\widetilde{D}_z$

		a/h			
		2	4	10	100
$w \times 10^{11}$ at $z = 0$	LD4	4.9113	30.029	582.06	4675300
	LD1	4.8087	29.852	579.26	4647300
	ED4	4.5047	28.591	573.25	4673900
	ED1	2.8575	18.488	423.29	3668700
	EDZ1	2.9117	20.153	498.04	4435100
	FSDT	2.8575	18.488	423.29	3668700
	CLT	0.58607	9.3884	364.43	2593400
σ_{xx} at $z = h/2$	LD4	3.2207	6.5642	32.771	3142.1
	LD1	3.5181	6.9995	34.256	3266.9
	ED4	2.4339	5.6978	31.785	3126.4
	ED1	2.0034	6.4471	37.374	3682.7
	EDZ1	2.0831	5.8424	32.946	3232.8
	FSDT	1.4836	5.9023	36.832	3682.1
	CLT	1.4722	5.8977	36.632	2606.9
σ_{xz} at $z = 0$	LD4	0.26995	0.68720	1.8540	18.832
$\Phi \times 10^3$ at $z = 0$	LD4	0.9103	6.1084	44.471	4580.2
	LD1	0.8597	6.0303	44.175	4552.7
	ED4	0.94157	6.1274	44.402	4568.9
	ED1	0.78657	2.6580	15.044	1470.3
	EDZ1	1.3901	6.3499	41.379	4171.8
	FSDT	0.78657	2.6580	15.044	1470.3
	CLT	0.38494	2.1095	14.366	1040.5
$\widetilde{D}_z \times 10^9$ at $z = h/2$	LD4	0.0256	0.0161	0.0139	0.0136
	LD1	−0.0662	−0.0880	−0.2853	−23.838
	ED4	0.0489	0.0353	0.0327	0.0324
	ED1	0.0834	0.0464	−0.1163	−18.729
	EDZ1	0.1496	0.1397	0.1372	0.1367
	FSDT	0.0615	0.0401	−0.1174	−18.729
	CLT	−0.0088	−0.0314	−0.1883	−13.311
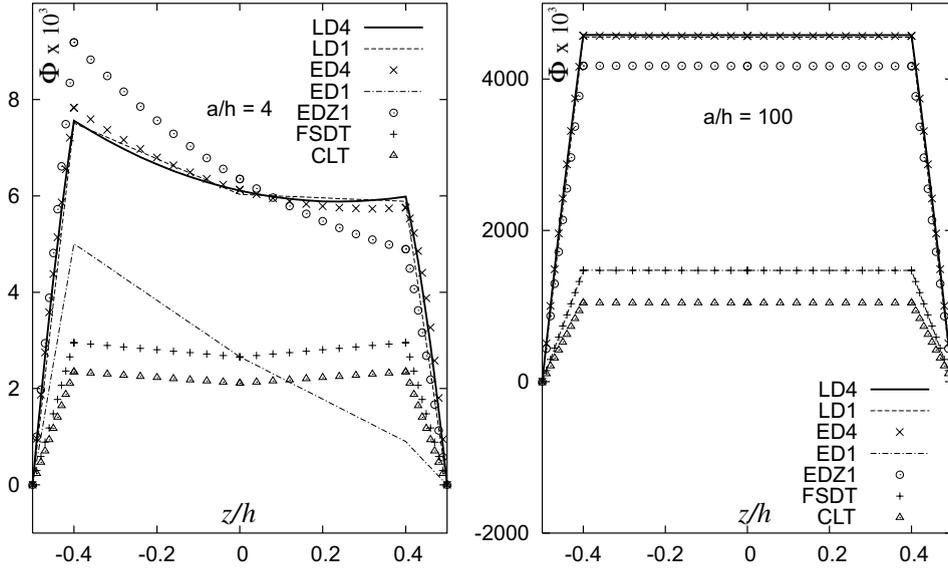
Fig. 13. Problem II, potential $\Phi \times 10^3$ vs. z/h for $a/h = 4$ and $a/h = 100$.

Table 10
Problem III, selected results for w, σ_{xx}, σ_{xz}, Φ and $\widetilde{D}_z$

		a/h			
		2	4	10	100
$w \times 10^{11}$ at $z = 0$	LD4	−1.7475	−1.4707	−1.3697	−1.3493
	LD1	−2.1030	−1.5962	−1.4297	−1.3971
	ED4	−4.4320	−3.5676	−3.2840	−3.2284
	ED1	−13.923	−14.107	−14.159	−14.171
	EDZ1	−13.583	−13.679	−13.706	−13.711
	FSDT	−13.923	−14.107	−14.159	−14.169
	CLT	0.1863	−0.1919	0.1916	0.1364
σ_{xx} at $z = h/2$	LD4	3.8162	1.1180	0.1680	−0.0246
	LD1	12.425	3.3433	0.5256	−0.0210
	ED4	8.5792	2.389	0.3687	−0.0269
	ED1	−4.206	−1.117	−0.1953	−0.0219
	EDZ1	1.2438	0.4308	0.0589	−0.0194
	FSDT	−0.8194	−0.2129	−0.0422	−0.0015
	CLT	−0.7329	−0.1931	−0.0394	−0.0102
σ_{xz} at $z = 0$	LD4	−0.0864	−0.0239	−0.0020	0.0000
Φ at $z = 0$	LD4	0.3330	0.4477	0.4910	0.4999
	LD1	0.3242	0.4468	0.4910	0.4999
	ED4	0.3343	0.4481	0.4911	0.4999
	ED1	0.3219	0.4461	0.4908	0.4999
	EDZ1	0.3335	0.4478	0.4910	0.4999
	FSDT	0.3219	0.4461	0.4908	0.4999
	CLT	0.3244	0.4470	0.4910	0.4999
$\widetilde{D}_z \times 10^9$ at $z = h/2$	LD4	−9.4085	−2.4184	−0.4168	−0.0370
	LD1	−5.2964	−1.3814	−0.2504	−0.0354
	ED4	−9.1127	−2.3523	−0.4068	−0.0369
	ED1	−3.8089	−0.9669	−0.1819	−0.0347
	EDZ1	−8.6524	−2.2360	−0.3879	−0.0367
	FSDT	−3.6667	−0.9566	−0.1816	−0.0347
	CLT	−3.2297	−0.8443	−0.1635	−0.0345
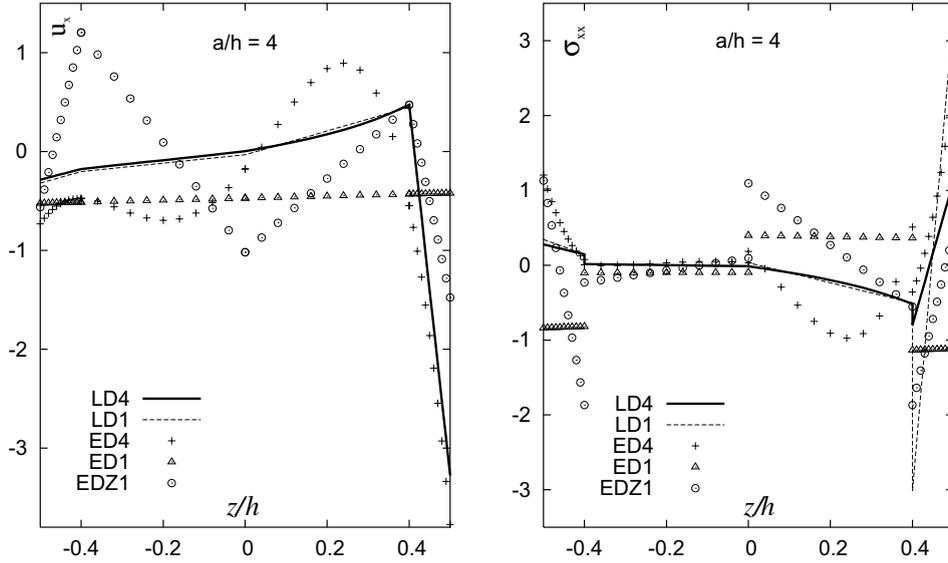
Fig. 14. Problem III, displacement $u_x \times 10^{11}$ and in-plane stress σ_{xx} vs. z/h for $a/h = 4$.

load on the top surface. In this case, the piezoelectric layers act passively as sensors for the actual deformation state of the structure. Thus, the main focus is put on the ability of the different models to represent the resulting electric field distribution, i.e. the potential values at the interfaces between piezoelectric layers and the structure. Fig. 13 shows thickness distributions of the potentials Φ for the cases $a/h = 4$ and $a/h = 100$. Independently from the thickness ratio, the low-order ESL theories fail to predict correctly the potential distribution, the error is in the range of 50%. The unsymmetric distribution in the thick plate case due to the influence of normal stress and shear can not be represented with CLT or FSDT. A remarkable improvement of the results in the case of the low order zig-zag theories (EDZ1) can be observed. Acceptable results can be achieved using high order ESL assumptions.

5.3.3. Problem III—actuator configuration

An overview of selected results for Problem III is given in Table 10. In this case an applied potential on the top surface of the plate is considered. In this configuration the upper piezoelectric layer is used as an actuator to impose a deformation on the whole plate. In all given models, the potential is assumed layer-wise which leads to a high accuracy of the electric variables. More interesting for the actuator configuration in comparison to the previous sensor case is the quality of the mechanical results. In Fig. 14 the thickness distributions of the in-plane displacement u_x and stress σ_{xx} for $a/h = 4$ are plotted. The actuation through the potential on the piezoelectric layer is a strongly localized effect. The dis-

placement shows a high gradient in this area and a sharp edge at the upper layer interface. It can be observed, that the ESL models have difficulties to represent this highly unsymmetric behavior. The two models ED4 and EDZ1 show a fairly good approximation in the piezoelectric layers but defer in the lower part of the laminate. The stresses, which are calculated dependently of the displacements reflect the errors of the displacement calculation. It can thus be concluded that ESL theories are not sufficient for a reliable calculation of the mechanical reaction to an electrical actuation.

6. Conclusion

The unified formulation for piezoelectric multilayered plates was derived and a closed-form solution found. It was demonstrated that the fourth order layer-wise model LD4 leads to the exact solution. On the base of this conclusion, the results of existing 3D solutions for three different problems were extended to additional thickness ratios. For all three problems a broad range of data for the different modelings included in the unified formulation is made available. Two issues were observed in a first comparative analysis: (1) For calculation of natural frequencies ESL models with moderate order of expansion yield results with acceptable accuracy. (2) The analysis of local responses that depend on the coupling between the electrical and mechanical systems requires a layer-wise description of the displacement or at least the separated modeling of the piezoelectric and the structural layers.

Appendix A. Arrays

A.1. Fundamental nuclei

Following abbreviations are used for the integrals in thickness direction:

$$\boldsymbol{E}_{\tau s} = \int_A F_\tau F_s \,\mathrm{d}z \quad \boldsymbol{E}_{\tau_z s} = \int_A \partial_z F_\tau F_s \,\mathrm{d}z$$

$$\boldsymbol{E}_{\tau s_z} = \int_A F_\tau \partial_z F_s \,\mathrm{d}z \quad \boldsymbol{E}_{\tau_z s_z} = \int_A \partial_z F_\tau \partial_z F_s \,\mathrm{d}z$$

$$K_{uu\,11}^{k\tau s} = \left(-\widetilde{C}_{11}^k \partial_x - 2\widetilde{C}_{16}^k \partial_x\partial_y - \widetilde{C}_{66}^k \partial_{yy}\right)E_{\tau s} + \widetilde{C}_{55}^k E_{\tau_z s_z}$$

$$K_{uu\,12}^{k\tau s} = \left(-\widetilde{C}_{16}^k \partial_{xx} - \left(\widetilde{C}_{12}^k + \widetilde{C}_{66}^k\right)\partial_x\partial_y - \widetilde{C}_{26}^k \partial_{yy}\right)E_{\tau s}$$
$$+ \widetilde{C}_{45}^k E_{\tau_z s_z}$$

$$K_{uu\,13}^{k\tau s} = \left(\widetilde{C}_{55}^k \partial_x + \widetilde{C}_{45}^k \partial_y\right)E_{\tau_z s} - \left(\widetilde{C}_{13}^k \partial_x + \widetilde{C}_{36}^k \partial_y\right)E_{\tau s_z}$$

$$K_{uu\,21}^{k\tau s} = \left(-\widetilde{C}_{16}^k \partial_{xx} - \left(\widetilde{C}_{12}^k + \widetilde{C}_{66}^k\right)\partial_x\partial_y - \widetilde{C}_{26}^k \partial_{yy}\right)E_{\tau s}$$
$$+ \widetilde{C}_{45}^k E_{\tau_z s_z}$$

$$K_{uu\,22}^{k\tau s} = \left(-\widetilde{C}_{66}^k \partial_{xx} - 2\widetilde{C}_{26}^k \partial_x\partial_y - \widetilde{C}_{22}^k \partial_{yy}\right)E_{\tau s} + \widetilde{C}_{44}^k E_{\tau_z s_z}$$

$$K_{uu\,23}^{k\tau s} = \left(\widetilde{C}_{45}^k \partial_x + \widetilde{C}_{44}^k \partial_y\right)E_{\tau_z s} - \left(\widetilde{C}_{36}^k \partial_x + \widetilde{C}_{23}^k \partial_y\right)E_{\tau s_z}$$

$$K_{uu\,31}^{k\tau s} = \left(\widetilde{C}_{13}^k \partial_x + \widetilde{C}_{36}^k \partial_y\right)E_{\tau_z s} - \left(\widetilde{C}_{55}^k \partial_x + \widetilde{C}_{45}^k \partial_y\right)E_{\tau s_z}$$

$$K_{uu\,32}^{k\tau s} = \left(\widetilde{C}_{36}^k \partial_x + \widetilde{C}_{23}^k \partial_y\right)E_{\tau_z s} - \left(\widetilde{C}_{45}^k \partial_x + \widetilde{C}_{44}^k \partial_y\right)E_{\tau s_z}$$

$$K_{uu\,33}^{k\tau s} = \left(-\widetilde{C}_{55}^k \partial_{xx} - 2\widetilde{C}_{45}^k \partial_x\partial_y - \widetilde{C}_{44}^k \partial_{yy}\right)E_{\tau s} + \widetilde{C}_{33}^k E_{\tau_z s_z}$$

$$\boldsymbol{K}_{ue}^{k\tau s}$$
$$= \begin{bmatrix} e_{15}^k\partial_x E_{\tau_z s} & e_{14}^k\partial_y E_{\tau_z s} & -(e_{31}^k\partial_x + e_{36}^k\partial_y)E_{\tau s_z} \\ e_{25}^k\partial_x E_{\tau_z s} & e_{24}^k\partial_y E_{\tau_z s} & -(e_{36}^k\partial_x + e_{32}^k\partial_y)E_{\tau s_z} \\ -(e_{15}^k\partial_{xx} + e_{25}^k\partial_x\partial_y)E_{\tau s} & -(e_{14}^k\partial_x\partial_y + e_{24}^k\partial_{yy})E_{\tau s} & e_{33}^k E_{\tau_z s_z} \end{bmatrix}$$

$$\boldsymbol{K}_{eu}^{k\tau s}$$
$$= \begin{bmatrix} -e_{15}^k\partial_x E_{\tau s_z} & -e_{25}^k\partial_x E_{\tau s_z} & -(e_{15}^k\partial_{xx} + e_{25}^k\partial_x\partial_y)E_{\tau s} \\ -e_{14}^k\partial_y E_{\tau s_z} & -e_{24}^k\partial_y E_{\tau s_z} & -(e_{14}^k\partial_x\partial_y + e_{24}^k\partial_{yy})E_{\tau s} \\ (e_{31}^k\partial_x + e_{36}^k\partial_y)E_{\tau_z s} & (e_{36}^k\partial_x + e_{32}^k\partial_y)E_{\tau_z s} & e_{33}^k E_{\tau_z s_z} \end{bmatrix}$$

$$\boldsymbol{K}_{ee}^{k\tau s} = \begin{bmatrix} \varepsilon_{11}^k\partial_{xx}E_{\tau s} & 0 & 0 \\ 0 & \varepsilon_{22}^k\partial_{yy}E_{\tau s} & 0 \\ 0 & 0 & -\varepsilon_{33}^k E_{\tau_z s_z} \end{bmatrix}$$

A.2. Closed-form solution

Fundamental nuclei for closed-form solution, restricted to orthotropic material.

$$\hat{K}_{uu\,11}^{k\tau s} = \left(\left(\alpha^2\widetilde{C}_{11}^k + \beta^2\widetilde{C}_{66}^k\right)E_{\tau s} + \widetilde{C}_{44}^k E_{\tau_z s_z}\right)$$

$$\hat{K}_{uu\,12}^{k\tau s} = \alpha\beta\left(\widetilde{C}_{12}^k + \widetilde{C}_{66}^k\right)E_{\tau s}$$

$$\hat{K}_{uu\,13}^{k\tau s} = \alpha\left(\widetilde{C}_{44}^k E_{\tau_z s} - \widetilde{C}_{13}^k E_{\tau s_z}\right)$$

$$\hat{K}_{uu\,21}^{k\tau s} = \alpha\beta\left(\widetilde{C}_{12}^k + \widetilde{C}_{66}^k\right)E_{\tau s}$$

$$\hat{K}_{uu\,22}^{k\tau s} = \left(\left(\alpha^2\widetilde{C}_{66}^k + \beta^2\widetilde{C}_{22}^k\right)E_{\tau s} + \widetilde{C}_{55}^k E_{\tau_z s_z}\right)$$

$$\hat{K}_{uu\,23}^{k\tau s} = \beta\left(\widetilde{C}_{55}^k E_{\tau_z s} - \widetilde{C}_{23}^k E_{\tau s_z}\right)$$

$$\hat{K}_{uu\,31}^{k\tau s} = \alpha\left(\widetilde{C}_{44}^k E_{\tau s_z} - \widetilde{C}_{13}^k E_{\tau_z s}\right)$$

$$\hat{K}_{uu\,32}^{k\tau s} = \beta\left(\widetilde{C}_{55}^k E_{\tau s_z} - \widetilde{C}_{23}^k E_{\tau_z s}\right)$$

$$\hat{K}_{uu\,33}^{k\tau s} = \left(\left(\alpha^2\widetilde{C}_{44}^k + \beta^2\widetilde{C}_{55}^k\right)E_{\tau s} + \widetilde{C}_{33}^k E_{\tau_z s_z}\right)$$

$$\hat{\boldsymbol{K}}_{ue}^{k\tau s} = \begin{bmatrix} \alpha e_{15}^k E_{\tau_z s} & 0 & -\alpha e_{31}^k E_{\tau s_z} \\ 0 & \beta e_{24}^k E_{\tau_z s} & -\beta e_{32}^k E_{\tau s_z} \\ \alpha^2 e_{15}^k E_{\tau s} & \beta^2 e_{24}^k E_{\tau s} & e_{33}^k E_{\tau_z s_z} \end{bmatrix}$$

$$\hat{\boldsymbol{K}}_{ee}^{k\tau s} = \begin{bmatrix} -\alpha^2\varepsilon_{11}E_{\tau s} & 0 & 0 \\ 0 & -\beta^2\varepsilon_{22}E_{\tau s} & 0 \\ 0 & 0 & -\varepsilon_{33}E_{\tau_z s_z} \end{bmatrix}$$

References

[1] Curie J, Curie P. Comptes Rendus 1880;91:294–5.
[2] Rao S, Sunar M. Piezoelectricity and its use in disturbance sensing and control of flexible structures: a survey. Appl Mech Rev 1994;47(4):113–23.
[3] Chopra I. State-of-the-art of smart structures and integrated systems. In: SPIE smart structures materials conference SPIE, vol. 2717, 1996. p. 20–62.
[4] Tani J, Takagi T, Qiu J. Intelligent materials systems: application of functional materials. Appl Mech Rev 1998;51(8):505–21.
[5] Sunar M, Rao S. Recent advances in sensing and control of flexible structures via piezoelectric materials technology. Appl Mech Rev 1999;52(1):1–16.
[6] Carrera E. Historical review of zig-zag theories for multilayered plates and shells. Appl Mech Rev 2003;56:287–308.
[7] Tiersten H. Linear piezoelectric plate vibrations. New York: Plenum; 1969.
[8] Mindlin R. High frequency vibrations of piezoelectric crystal plates. Int J Solids Struct 1972;8:895–906.
[9] Yang J, Yu J. Equations for laminate piezoelectric plates. Arch Mech 1993;45:653.
[10] Mitchell J, Reddy J. A refined hybrid plate theory for composite laminates with piezoelectric laminae. Int J Solids Struct 1995;32(16):2345–67.
[11] Reddy J. Mechanics of laminated composite plates: theory and analysis. CRC Press Inc.; 1996.

[12] Benjeddou A, Deü J-F. A two-dimensional closed-form solution for the free-vibrations analysis of piezoelectric sandwich plates. Int J Solids Struct 2001;39:1463–86.

[13] Touratier M, Ossadzow-David C. Multilayered piezoelectric refined plate theory. AIAA J 2003;41(1):90–9.

[14] Saravanos D, Heyliger P. Mechanics and computational models for laminated piezoelectric beams, plates and shells. Appl Mech Rev 1999;52(10):305–20.

[15] Benjeddou A. Advances in piezoelectric finite element modeling of adaptive structural elements: a survey. Comput Struct 2000;76(1–3):347–63.

[16] Carrera E. A class of two dimensional theories for multilayered plates analysis, Atti Accademia delle Scienze di Torino. Mem Sci Fis 1995;19–20:49–87.

[17] Carrera E. Developments, ideas and evaluations based upon Reissner's mixed variational theorem in the modeling of multilayered plates and shells. Appl Mech Rev 2001;54(4):301–29.

[18] Carrera E. Theories and finite elements for multilayered, anisotropic composite plates and shells. Arch Comput Methods Eng State of the art Rev 2002;9:87–140.

[19] Carrera E. Theories and finite elements for multilayered plates and shells: a unified compact formulation. Arch Comput Methods Eng, State of the art Rev 2003;10(3):215–96.

[20] Murakami H. Laminated composite plate theory with improved in-plane response. J Appl Mech 1986;53:661–6.

[21] A.N.S. Institute, IEEE standard on piezoelectricity.

[22] Heyliger P, Saravanos D. Exact free-vibration analysis of laminated plates with embeded piezoelectric layers. J Acoust Soc Am 1995;98(3):1547–57.

[23] Heyliger P. Static behavior of laminated elastic/piezoelectric plates. AIAA J 1994;32(12):2481–4.